

Cluster mass estimation from lens magnification

Eelco van Kampen

Royal Observatory Edinburgh, Blackford Hill, Edinburgh EH9 3HJ

Theoretical Astrophysics Center, Juliane Maries Vej 30, DK-2100 København Ø, Denmark, eelco@tac.dk

Accepted ... Received ...; in original form ...

ABSTRACT

The surface mass density of a cluster of galaxies, and thus its total mass, can be estimated from its lens magnification. The magnification can be determined from the variation in number counts of its background galaxies. In the weak lensing approximation the surface mass density is a linear function of the magnification. However, most observational data is concentrated in the central parts of clusters, so one needs to go beyond the weak lensing approximation, and consider the lens shear as well, which is unknown from the variation in number counts alone. Our approach is to look for approximate relations between the lens shear and other lens properties in this strong lensing regime.

Such relations exist for simple analytical cluster models, like the isothermal sphere, but are not generally a good description of observed or simulated galaxy clusters. We therefore study the lensing properties of a catalogue of numerical cluster models in order to find the best possible approximation for the shear which still allows straightforward determination of the surface mass density. We show that by using such an approximation one can fairly well reconstruct the surface mass distribution from the magnification alone. The approximations are tested using clean magnification maps obtained directly from simulated clusters, and also using lensed mock background galaxy distributions in order to estimate the intrinsic uncertainties of the method. We demonstrate that the mass estimated using the weak lens magnification approximation is usually at least twice the true mass. We illustrate our technique on existing data, and show that the resulting masses compare well to other estimates.

Key words: cosmology: theory – dark matter – large-scale structure of Universe – gravitational lensing

1 INTRODUCTION

A rich cluster of galaxies acts as a gravitational lens on the galaxy distribution behind it. This simple fact can be used to derive a great deal about both the lensing cluster as well as the background galaxy population (eg. Schneider, Ehlers & Falco 1992; Fort & Mellier 1994; Kaiser 1996). In this paper we deal with methods that exploit the variation in galaxy number counts caused by the lensing cluster to obtain properties of that cluster, for example its total mass. Broadhurst, Taylor & Peacock (1995, BTP from here on) have shown how this variation in number counts of background galaxies depends on the lens magnification, and how to best obtain the latter from the former.

In order to obtain a total mass for the lens, or a mass distribution, one has to somehow derive the surface mass density from the lens magnification. BTP use the weak lens approximation to relate the two directly. However, this approximation is only valid in the outskirts of clusters, while

most of the observational data is restricted to the central parts of clusters, where lensing is strong. We therefore need to go beyond the weak lensing approximation to realistically estimate the cluster surface mass density in this strong lensing regime. This means that besides the magnification one needs the shear distribution in order to obtain the lens convergence, and thus the surface mass density of the lens.

There are various ways of obtaining the shear distribution from observations, like the method devised by Kaiser & Squires (1993) that utilizes the shearing of the background galaxy images to estimate the tangential shear component (but not the radial one). This method also provides a way to estimate the surface mass density, save a constant. The problem of this unknown constant, dubbed the ‘sheet-mass degeneracy’ (Gorenstein, Falco & Shapiro 1988), prevents absolute mass measures, although the edges of the observed field can be used to put a lower limit on the mass by requiring it to be positive everywhere. Furthermore, Kaiser & Squires (1993) again assume weak lensing. Extensions

to these methods in order to break this degeneracy and/or consider the strong lensing regime have been devised by, amongst others, Schneider & Seitz (1995), Kaiser (1995), Schneider (1995) and Bartelmann et al. (1996). The reliability of these and other shear methods has been discussed by Bartelmann (1995) and Wilson, Cole & Frenk (1996).

However, an approximation that relates the shear field to either the magnification or the convergence field allows one to obtain an absolute measure for the convergence, and thus the surface mass density, from the magnification alone. This also provides a mass estimate that is independent from other methods. Observationally, measuring the shapes of galaxies is more difficult than just counting them. Thus, a route to the cluster mass from the lens magnification alone is a major advantage: ground-based observations are sufficient, as imaging of the galaxies is not required.

We use a sample of numerical galaxy cluster models (van Kampen & Katgert 1997) to find heuristic relations between lens shear and lens convergence (or lens magnification). We also consider some relations that have an underlying assumption about the physical state of the lens, like isotropy.

In order to find the maximum performance of the estimators that correspond to such approximations, we test how well one can estimate the surface mass density from just the magnification map, as obtained directly from a numerical cluster model. Subsequently, we test how well the estimators work on magnification maps that were obtained from lensed mock background galaxy distributions. We roughly follow the same procedures as an observer would for an observed galaxy distribution, thus mimicking most of the problems involved in the application of the method.

Recently, Fort, Mellier & Dantel-Fort (1997) and Taylor et al. (1998) showed that a depletion in number counts can clearly be observed. Fort et al. (1997) showed this most convincingly for the cluster CL 0024+1654. They did not try to estimate the cluster surface mass density or the total mass, however. Taylor et al. (1998) did estimate a mass for A1689, and found it to be consistent with other mass measures.

The paper is outlined as follows: in Section 2 we sketch the path from observed number counts to estimated cluster properties. The necessary approximations and methods are introduced in Section 3, and tested on simulated data in Section 4. We apply the technique to published data in the literature in Section 5.

2 THE LENS MAGNIFICATION METHOD

2.1 The thin lens approximation

We summarize the main features of the thin lens approximation, following Schneider, Ehlers & Falco (1992) and Bartelmann & Weiss (1994), paying attention to those elements that are important for this paper. For properly renormalized mass and length scales (see Bartelmann & Weiss 1994 for details), the lens equation becomes

$$\mathbf{y} = \mathbf{x} - \alpha(\mathbf{x}), \quad (1)$$

where \mathbf{x} and \mathbf{y} represent the lens and source planes respectively, and α is the deflection angle, being the gradient of the lens potential ψ , given by

$$\alpha(\mathbf{x}) = \nabla\psi(\mathbf{x}) = (\kappa * \mathbf{K})(\mathbf{x}). \quad (2)$$

Here we have introduced the lens convergence κ , being the dimensionless surface mass density $\Sigma(\xi_0\mathbf{x})$ of the lens (where ξ_0 scales the dimensionless \mathbf{x} to a dimensional quantity):

$$\kappa(\mathbf{x}) \equiv \Sigma(\xi_0\mathbf{x})/\Sigma_{\text{cr}}, \quad (3)$$

and the kernel

$$\mathbf{K}(\mathbf{x}) \equiv \frac{1}{\pi} \frac{\mathbf{x}}{|\mathbf{x}|^2} \quad (4)$$

with which κ is convolved to obtain the deflection angle. The *critical* surface mass density Σ_{cr} plays an important rôle in lensing theory. It is defined as

$$\Sigma_{\text{cr}} \equiv \rho_{\text{cr}} \frac{c}{3H_0} f(z_{\text{d}}, z_{\text{s}}), \quad (5)$$

where ρ_{cr} is the critical density of the background universe, and $f(z_{\text{d}}, z_{\text{s}})$ a function of the lens redshift z_{d} and the source redshift z_{s} , whose expression depends on the geometry of the universe, i.e. the cosmological model (see Schneider et al. 1992, ch. 5). From the deflection angle we can calculate the lens magnification and shear through the Jacobian \mathbf{A} of the lens mapping:

$$\mathbf{A}(\mathbf{x}) = \left(\frac{d\mathbf{y}}{d\mathbf{x}} \right) = \mathbf{I} - \frac{d\alpha(\mathbf{x})}{d\mathbf{x}}. \quad (6)$$

The lens magnification μ is obtained from its determinant:

$$\mu^{-1}(\mathbf{x}) = \det \mathbf{A}(\mathbf{x}) = A_{11}A_{22} - A_{12}A_{21}. \quad (7)$$

The lens shear consists of the two trace-free components

$$\gamma_1(\mathbf{x}) = \frac{1}{2}(A_{22} - A_{11}), \quad \gamma_2(\mathbf{x}) = -A_{12} = -A_{21}, \quad (8)$$

with the total shear given by

$$\begin{aligned} \gamma^2 &= \gamma_1^2 + \gamma_2^2 = \frac{1}{4}(A_{22} - A_{11})^2 + A_{12}A_{21} \\ &= \frac{1}{4}(A_{11} + A_{22})^2 - \mu^{-1} \end{aligned} \quad (9)$$

The convergence can also be expressed in terms of \mathbf{A} through the Poisson equation for the lensing potential:

$$\kappa(\mathbf{x}) = \frac{1}{2}\nabla^2\alpha = 1 - \frac{1}{2}A_{11} - \frac{1}{2}A_{22}. \quad (10)$$

We can thus relate the three main lensing properties:

$$\mu^{-1} = (1 - \kappa)^2 - \gamma^2. \quad (11)$$

2.2 Cluster mass estimation from variations in number counts

We sketch the whole path, in three distinctive stages, from observed number counts to estimated cluster properties, notably the total mass. Besides describing the method, we indicate where we need to make assumptions.

2.2.1 Variation in number counts to magnification

The presence of a lens gives rise to a variation in the number counts of background galaxies (BTP). For galaxies counted up to a magnitude limit m_{lim} , we denote this variation as N/N_0 , where N_0 is the average galaxy number count for the field. Assuming that the integral luminosity function of these galaxies can for $m < m_{\text{lim}}$ be approximated by a power-law with slope S , the magnification μ can be calculated from N/N_0 and a maximum-likelihood analysis of

the background redshift distribution (BTP), taking into account the clustering of background galaxies which confuses the lensing signal (Taylor & Dye 1998). In case no redshift information is available for the background galaxies, an estimate for the absolute value of μ is given by

$$|\mu_{\text{est}}| = (N/N_0)^\beta, \text{ with } \beta = (2.5S - 1)^{-1}. \quad (12)$$

In most cases β is negative, i.e. we observe a depletion in number counts due to the presence of the cluster. Note that we can only measure the absolute value of μ , so we have to set its sign, the image parity, by hand.

Although the feasibility of actually obtaining μ from observational data is an interesting topic for discussion, the issue of this paper is how to proceed from the magnification to the properties of the lensing cluster. We therefore assume for the remainder of this paper that one can reliably measure the lens magnification, as it has been shown to be detectable (Fort, Mellier & Dantel-Fort 1997; Taylor et al. 1998).

2.2.2 Magnification to convergence

As is obvious from eq. (11), in order to obtain κ one needs to know both the lens magnification and shear. As the lens shear can be found from the distortion of the shapes of the background galaxies (Kaiser & Squires 1993), one could, in principle, combine this with the magnification found from the variation in number counts to calculate the convergence. However, here we like to use the latter as an *independent* determination of the convergence, as one can also derive κ , save a constant, directly from the lens shear (Kaiser & Squires 1993). Just detecting galaxies is also easier than obtaining their shapes, can be done in larger numbers, and from the ground. In order to get κ from the lens magnification alone, we need to make assumptions about the shear field. We do this by finding approximate relations for simulated clusters, which have known lensing properties. Once we have found a relation between the shear and either the magnification or the convergence, we can also go straight from the variation in number counts to an estimate for the convergence.

2.2.3 Convergence to projected cluster mass and other properties

The convergence of a lens depends on the redshift of the background galaxy being lensed, so for a distribution of background galaxies one finds a weighted average over convergences for each of these galaxies. In order to translate this convergence to a surface mass density we just multiply by Σ_{cr} for an *effective* source redshift, which depends on the redshift distribution adopted. The total projected mass is then found by integration over the surface mass density.

Many other methods for cluster mass estimation give 3D masses. We can derive these using a relation between 2D and 3D masses for the model cluster catalogue of van Kampen & Katgert (1997), which is given as a fit to the scatter plot for all models (van Kampen 1998):

$$\frac{M_{3\text{D}}}{M_{2\text{D}}} = 0.56 \tan^{-1} \left(\frac{R}{0.14h^{-1}\text{Mpc}} \right). \quad (13)$$

The scatter around this relation is fairly large for small R , due to substructure along the line-of-sight, but less than 10 per cent for $R > 0.4h^{-1}\text{Mpc}$ (van Kampen 1998).

3 FINDING AN OPTIMAL CONVERGENCE ESTIMATOR

3.1 General strategy

The convergence κ of a lens, from which we can obtain its mass, is not just a function of the lens magnification μ that we measure, but also of its lens shear γ (see eq. 11). One way to eliminate the dependence on γ is to find an approximate relation between γ and κ . This can be done by looking more closely at the Jacobian of the lens mapping, \mathbf{A} . All three main lensing properties are a function of two or more of its components. One can therefore try to statistically relate these components to each other. For example, if we assume that $A_{11} = A_{22}$, and both A_{12} and A_{21} vanish, we have $\gamma = 0$ and $\mu^{-1} = (\kappa - 1)^2$ (discussed in more detail below).

Another approach is to start from eq. 11, and assume an arbitrary local relation $\gamma(\kappa)$, i.e.

$$\mu^{-1}(\kappa) = (1 - \kappa)^2 - \gamma^2(\kappa). \quad (14)$$

For a typically aspherical and clumpy cluster, the convergence has a strong dipole component, while the shear is dominated by a quadrupole component. In other words, only specific lensing potentials will satisfy such a relation exactly. However, such a relation can be a good approximation for averaged quantities, like radial profiles, for example. Also, when these functions are smoothed significantly, as is often the case for observational data, approximate local relations should exist.

The assumption of locality of the shear allows many possible specific approximations, so the aim is to select either physically motivated $\gamma(\kappa)$, or a $\gamma(\kappa)$ that leads to a relation between μ and κ which is easily invertible, and therefore applicable to observations. We use a representative sample of cluster models to find such a relation, by simply investigating how shear and convergence relate to each other for these models.

One problem we will always have to deal with is that of image parity, the sign of the lens magnification, as we can only obtain $|\mu|$ from the observed number counts, and have to make an educated guess about this parity. In the general case we have a second parity as well, as the magnification is a quadratic function of κ and γ . In looking for a local relation between κ and γ we should therefore try to minimize the range of μ for which we have to set parities.

In devising approximations we need to take care that the shear γ remains real for all μ . Furthermore, we set $\mu^{-1}(0) = 1$, i.e. for $\kappa \rightarrow 0$ we also have $\gamma \rightarrow 0$, which corresponds to saying that the cluster is isolated.

The various possibilities, along with their physical interpretation, are discussed below. Both κ and γ are labelled to denote the approximation made, while μ and N/N_0 appear unindexed, as we consider them to be observed functions for the sake of this paper. We first consider approximations with just one parity.

3.2 Estimators with one parity

Estimators with only one parity which also have physical shear distributions are special cases of eq. (11): the expression $(\kappa - 1)^2 - \gamma^2$ is allowed to have a sign uncertainty, but its associated parity should be the same as that of $|\mu|$ in

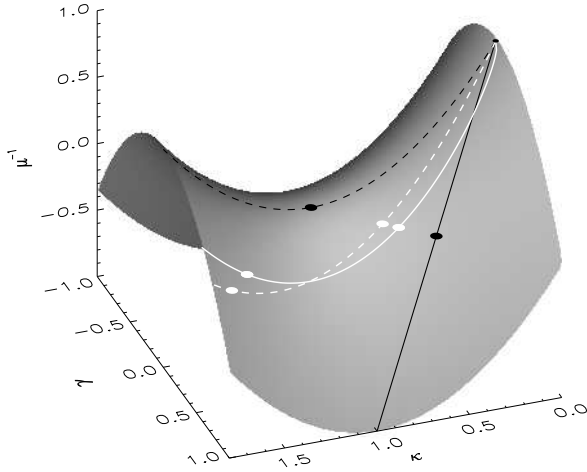


Figure 1. Lens magnification μ^{-1} as a function of convergence κ and shear γ . Several approximations relating κ and γ locally are indicated as lines on the surface, where black lines indicate the one-parity approximations $\gamma = 0$ (dashed line) and $\gamma = \kappa$ (solid line), described in Section 3.2, and white lines the two-parity approximations $\gamma \propto \kappa$ (dashed line) and $\gamma \propto \kappa^{1/2}$ (dotted line), described in Section 3.3. The caustics are indicated by large dots.

order to effectively have one parity only. This means that the following simple possibilities remain:

$$\begin{aligned} \mu^{-1} &= (\kappa - 1)^2 & (\gamma = 0) \\ \mu^{-1} &= 1 - 2\kappa & (\gamma = \kappa) \\ \mu^{-1} &= \gamma^2 & (\kappa = 0) \end{aligned} \quad (15)$$

If we try $\mu^{-1} = (\kappa - q)^2$, then $\gamma^2 = q^2 - 1 + 2(1 - q)\kappa$, which is only positive definite for $q = 1$, the first possibility listed above. The last possibility is not very likely in reality, obviously.

In Fig. 1 we have plotted μ^{-1} as a function of both κ and γ . On this surface of possible $(\kappa, \gamma, \mu^{-1})$, we have drawn the $\gamma = \kappa$ (solid black line) and $\gamma = 0$ (dashed black line) approximations. This shows why only these two remain when we require the one parity approximations to go through $(\kappa, \gamma, \mu^{-1}) = (0, 0, 1)$.

More complicated functions of $\mu^{-1}(\kappa)$ can be proposed, of course, which start at $(0, 0, 1)$, and cross the $\mu^{-1} = 0$ plane only once. But all of these also lead to complicated (and probably multi-valued) expressions for $\gamma(\kappa)$, and, more importantly, inversion of $\mu^{-1}(\kappa)$ becomes less straightforward.

3.2.1 No shear: $\gamma = 0$

The first of the two one-parity approximations is also the simplest: we forget about shear altogether, which corresponds to treating the cluster as a uniform sheet of matter. This means that we set $A_{11} = A_{22}$, and $A_{12} = A_{21} = 0$. Setting $\gamma = 0$, the estimator is easily derived from eq. (11):

$$\kappa_0 = 1 - \mathcal{P}|\mu|^{-1/2} = 1 - \mathcal{P}(N/N_0)^{-\beta/2}, \quad (16)$$

where \mathcal{P} is the image parity, i.e. the sign of μ . In this approximation there is one critical line, at $\kappa = 1$, which separates the two parity regimes: $\mathcal{P} = 1$ for $\kappa < 1$, and $\mathcal{P} = -1$ for $\kappa > 1$.

For observational data κ is of course a-priori unknown, but the position of the critical line can usually be guessed from the occurrence of giant arcs, or the position of a significant dip in the number counts, most easily in number counts in spherical bins, but also in 2D maps.

3.2.2 Isotropic approximation: $\gamma = \kappa$

BTP argue that if the fluctuations around the mean lensing potential are reasonably isotropic, that :

$$\langle (1 - A_{11})^2 \rangle \approx \langle (1 - A_{22})^2 \rangle \approx \langle (A_{12})^2 \rangle \quad (17)$$

(note that there is a typographical error in their eq. 19). If we make this exact, i.e. $1 - A_{11} = 1 - A_{22} = A_{12} = A_{21}$, we find that $\gamma_1 = 0$, $\gamma_2^2 = \gamma^2 = \kappa^2 = (1 - A_{11})^2$ etc., and $\mu^{-1} = 1 - 2\kappa$.

So, assuming that the shear is equal to the convergence results in the estimator

$$\kappa_1 = \frac{1}{2} - \frac{1}{2}\mathcal{P}|\mu^{-1}| = \frac{1}{2} - \frac{1}{2}\mathcal{P}\left(\frac{N}{N_0}\right)^{-\beta}, \quad (18)$$

where \mathcal{P} is again the image parity. The critical line is now assumed to be at $\kappa = 1/2$, so this estimator automatically gives a smaller mass than the shearless mass estimator which assumes $\kappa = 1$ at the critical line. This makes physical sense, as there is now a shear contribution to the lensing, while in the shearless case κ has to account for all the magnification.

3.2.3 Linear approximation

All approximations discussed so far can be linearized to the simple form

$$\kappa_{\text{lin}} = \frac{1}{2}(\mu - 1) = \frac{1}{2}\left(\frac{N}{N_0}\right)^{\beta}, \quad (19)$$

a form used by BTP and others. This approximation is obviously useful for $\mu \approx 1$ only, corresponding to small κ , i.e. the outskirts of clusters. However, most observational data is restricted to the core of the cluster only, because of the limited field of view (for the *Hubble Space Telescope* for example), or because the data was taken for other reasons. This renders the linear approximation quite useless for our purposes. We will show it for reference only in the remainder of this paper. Note that the linear approximation has no critical curves and no parity changes, as μ , being proportional to κ , will never become zero; it will only increase towards the centre.

3.3 Heuristic estimators

A typical cluster will be aspherical and clumpy, which means that the simple approximations described above will not hold. In fact, an exact local relation between the lens convergence and shear is not expected to exist when the cluster is not spherical, as the convergence will generally have a strong dipole moment, while the shear is dominated by a quadrupole component. So we need to find a simple function which relates κ and γ on average.

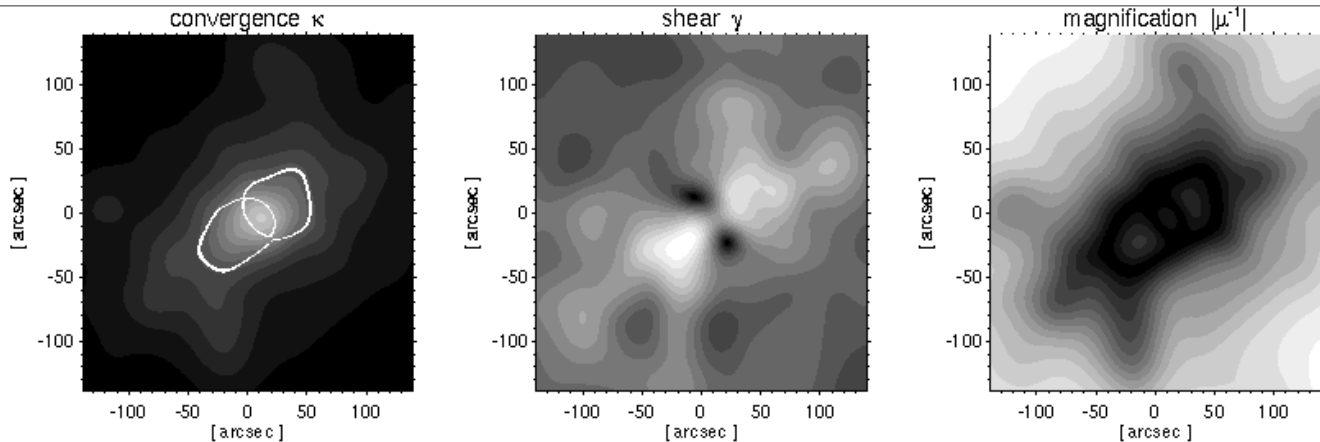


Figure 2. An example of the lens convergence, shear, and magnification for a simulated galaxy cluster (the fourth entry in Table 1). The convergence κ was obtained from an N-body simulation using adaptive window smoothing (see text for details). The shear γ and magnification μ were obtained from κ using the thin lens approximation.

Table 1. Properties of the four cluster models used for some of the Figures. The richness measure C_{ACO} is defined by Mazure et al. (1995), the parameter c is part of the heuristic estimator described in Section 3.3.2, z_{d} and z_{s} are the redshifts of the lens and the background galaxies respectively, whereas the cosmological parameter σ_8 determines how evolved the clusters are.

| no | σ_8 | Mass [$10^{15}M_{\odot}$] | $\sigma_{\text{v,l.o.s.}}$ [km s^{-1}] | C_{ACO} | z_{d} | z_{s} | c |
|----|------------|--------------------------------|--|------------------|----------------|----------------|------|
| 9 | 0.54 | 0.89 | 1061 | 109 | 0.2 | 0.8 | 0.85 |
| 13 | 0.63 | 1.58 | 1140 | 153 | 0.4 | 2.0 | 0.80 |
| 41 | 0.79 | 2.67 | 1591 | 174 | 0.2 | 0.8 | 0.76 |
| 41 | 0.92 | 2.91 | 1563 | 169 | 0.4 | 2.0 | 0.70 |

3.3.1 Numerical cluster models

A fruitful approach is to look at numerical cluster models, and find a local relation between κ and γ by looking at scatter-plots of these two quantities from the pixels of the convergence and shear maps of model clusters. This is useful only when we look at a fair sample of clusters models, which is representative for the variety of clusters found on the sky. For this purpose we use the catalogue of high-resolution cluster models of van Kampen & Katgert (1997), which was constructed to mimic an observed sample (Mazure et al. 1995; Katgert et al. 1995).

The individual cluster models were built using a dissipationless N-body code which was supplemented with a recipe for galaxy formation and merging (van Kampen 1994, 1997), which makes it possible to get Abell cluster properties like richness. A groups of particles that collapses into a virialized group with a mass corresponding to that of a galaxy halo is, during the simulation run, replaced by a single, massive ‘galaxy particle’. However, brightest cluster galaxies like cD’s and gE’s are *not* replaced by single particles. For the lensing properties of their parent cluster this is important, as both the core and the substructure of the cluster should be modelled with sufficient resolution (Bartelmann & Weiss

1994; Bartelmann, Steinmetz & Weiss 1995). We adopted a Plummer softening parameter of $40h^{-1}$ kpc (comoving), which is adequate for our purposes; see van Kampen (1994) for a more comprehensive discussion on resolution issues connected to the numerical simulation technique. Note that the resolution of the *projected* density distribution will automatically be higher. Therefore, more important is the use of adaptive window smoothing (see below), which retains that resolution as much as possible during the smoothing which is necessary for the calculation of the lens properties, since we use the thin lens approximation.

We use 29 cluster models that constitute a complete sample for richness $C_{\text{ACO}} > 75$ (the entries in boldface in Table 1 of van Kampen & Katgert 1997). Please refer to Mazure et al. (1995) for the definition of the richness parameter C_{ACO} . The 29 clusters were simulated for the standard Cold Dark Matter scenario, and have $\sigma_8 = 0.63$ when put at a redshift $z_{\text{D}} = 0.4$. However, we have also selected four specific cluster models, with a range in mass, σ_8 , and other properties relevant for lensing, for demonstrating the various methods and tests. The least massive of these models we may consider to be a ‘weak’ lens, while the most massive one is a ‘strong’ lens with both caustic lines present for most source redshifts. Some of the properties of these four models, and the redshift they are put at, are listed in Table 1. The cluster number relates to the entry in the catalogue of cluster models of van Kampen & Katgert (1997), where more properties of these models can be found.

3.3.2 Obtaining the lens properties of simulated galaxy clusters

We obtain the surface mass density (and thus the convergence) from the numerical models using adaptive window smoothing (Silverman 1986), with an initial (Gaussian) smoothing length of $0.25h^{-1}$ Mpc. This results in having a smoothing length of $0.05h^{-1}$ Mpc in the centre of the cluster models (which is identical to that used by Bartelmann & Weiss (1994) for their cluster models), and $1.0h^{-1}$ Mpc in the outskirts. This provides sufficient resolution for the lens mapping. For example, giant arcs are formed as expected

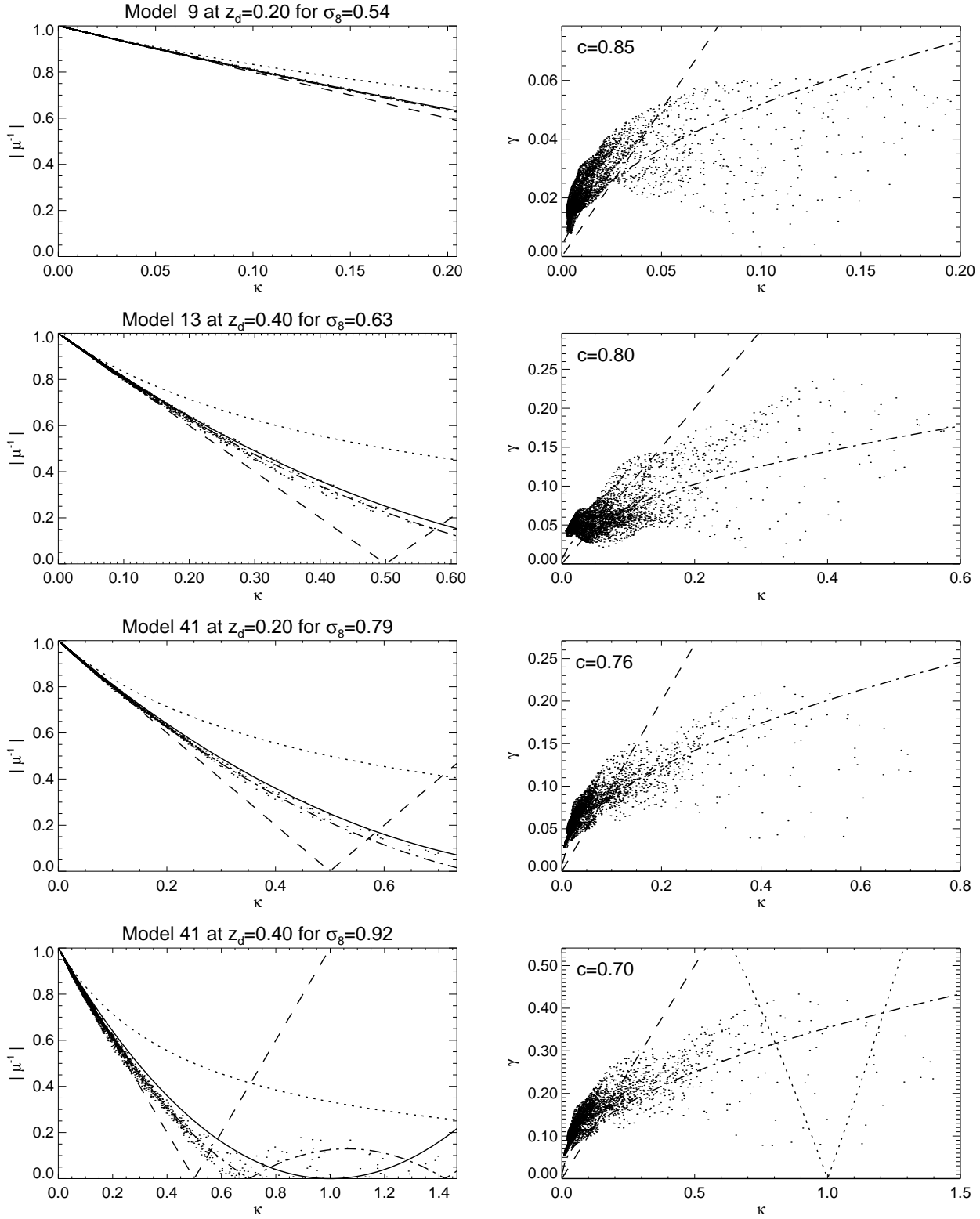


Figure 3. The left column shows scatter plots of the lens magnification μ versus the lens convergence κ , with corresponding plots of the lens shear γ versus κ , for the four clusters listed in Table 1. The parameter c for the $\gamma \propto \kappa^{1/2}$ estimator (dot³-dashed line) was fitted using the κ - γ plots, and is annotated in the right hand panels. Solid lines correspond to the $\gamma = 0$ approximation, dashed lines are for $\gamma = \kappa$, and dotted lines indicate the weak (i.e. linear) lens approximation.

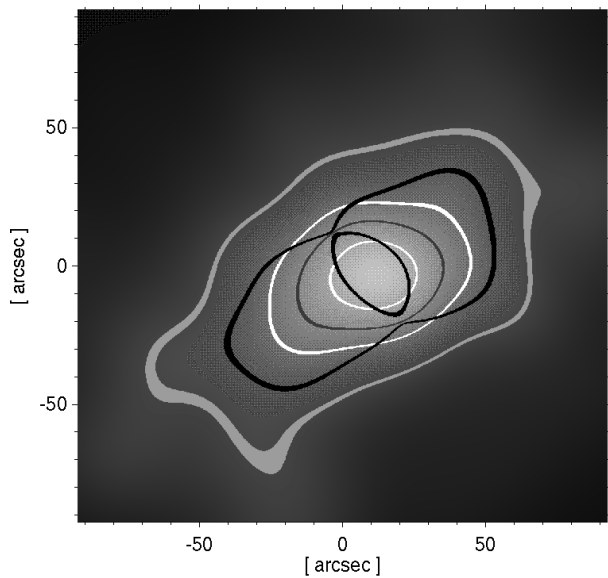


Figure 4. Comparison of the shear approximations in terms of their caustic lines. Show is the lens convergence for a massive clusters (the fourth entry of Table 1), with its true caustic lines (black curves) and the caustic lines corresponding to these approximations superimposed. White curves are for the assumption that $\gamma \propto \kappa^{1/2}$, dark grey curves for $\gamma = 0$, and light grey ones for $\gamma = \kappa$.

(van Kampen 1996). The lens shear and magnification are calculated using the thin lens approximation, as outlined in Section 2.1, with the convolution in eq. (2) done by Fast Fourier Transforms. All lens properties are calculated on a 1024×1024 grid which measures $4h^{-1}$ Mpc on a side. As an example we show these maps for the fourth cluster of Table 1 in Fig. 2, along with its caustics.

In Fig. 3 we plot, for the cluster models listed in Table 1, the absolute magnification $|\mu|$ versus the convergence κ , and the lens shear γ versus κ , as scatter plots. For clarity we plot just one out of every 250 pixels for each calculated map. We use these scatter plots to look for approximate relations between the lens properties.

3.3.3 $\gamma \propto \kappa^{1/2}$

The heuristic approach should preferably lead to simple approximations which can be applied to observed data in an unambiguous way. There will be two caustic lines, which means that two parities have to be set, so the approximation should preferably have only a small range of μ for which parities need to be set.

Studying Figs. 3, one gets the impression that, on average, γ is proportional to $\kappa^{1/2}$. This assumption leads to a well-behaved relation between $|\mu|$ and κ , which is also invertible. In general, if we assume

$$\gamma = [(c + c^{-1} - 2)\kappa]^{1/2}, \quad (20)$$

with $0 < c < 1$ (by convention), then

$$\mu^{-1} = (\kappa - c)(\kappa - c^{-1}). \quad (21)$$

This implies that there are two κ 's for each μ , but as we measure N/N_0 , we can only obtain $|\mu|$, which can correspond

to four different values of κ .

The estimator for κ , given $|\mu|$, is then

$$\kappa_c = \frac{c + c^{-1}}{2} - \mathcal{S} \left[\left(\frac{c + c^{-1}}{2} \right)^2 - \mathcal{P} |\mu|^{-1} - 1 \right]^{1/2}, \quad (22)$$

where \mathcal{P} is the lens parity, i.e. the sign of μ , while the new parity \mathcal{S} indicates which side of the minimum we are: it is the sign of $\kappa_{\min} - \kappa$, and switches sign around $\mu = \mu_{\min}$. These two minima are

$$\kappa_{c,\min} = (c + c^{-1})/2, \quad \mu_{\min} = \left(\frac{c + c^{-1}}{2} \right)^2 - 1. \quad (23)$$

Note that μ_{\min} is a local *maximum* for $|\mu_{\min}|$. Also, one recovers the $\gamma = 0$ approximation when $c = 1$.

The two critical lines are at $\kappa = c$ and $\kappa = c^{-1}$, as is obvious from eq. (21). We compare these critical lines to the true critical lines in Fig. (4), for a fairly massive cluster with central κ larger than one. For comparison, the critical lines corresponding to the $\gamma = 0$ and $\gamma = \kappa$ estimators are shown as well, in dark grey and light grey colours respectively.

Combining Eqs. (9), (10) and (20), we see that this approximation corresponds to assuming

$$A_{12}A_{21} = \frac{(c-1)^2}{2c} (2 - A_{11} - A_{22}) - \frac{1}{4}(A_{22} - A_{11})^2. \quad (24)$$

In order to solve this equation, we need to make a further assumption for A_{11} , A_{22} , and A_{12} (which is equal to A_{21}).

We can assume spherical symmetry, i.e. $\kappa = \kappa(x)$, but unfortunately, as shown in Appendix A, there exists no spherical solution for which $\gamma = [(c + c^{-1} - 2)\kappa]^{1/2}$. However, the Plummer potential, which can be written as

$$\phi(\theta) = \phi_0 \ln(\theta_c^2 + \theta^2), \quad (25)$$

where $\phi_0 = M\theta_c^2/2\pi R_c^2 \Sigma_{\text{cr}}$, does show this behaviour for $\theta > \theta_c$, where θ is the angular distance from the centre of the cluster, θ_c the angular core radius, Σ_{cr} the critical surface mass density as defined in eq. (5), and $R_c = \theta_c D_L$ its corresponding physical core radius, where D_L is the angular diameter distance from the lens to the observer. For this potential

$$\kappa(\theta) = 2\phi_0 \frac{\theta_c^2}{(\theta^2 + \theta_c^2)^2}, \quad \text{and} \quad \gamma(\theta) = 2\phi_0 \frac{\theta^2}{(\theta^2 + \theta_c^2)^2} \quad (26)$$

(Kochanek and Blandford 1991), which gives the following relation between κ and γ :

$$\gamma = \kappa_0 \kappa^{1/2} - \kappa = \kappa^{1/2} (\kappa_0^{1/2} - \kappa^{1/2}), \quad (27)$$

where $\kappa_0 = \kappa(0) = 2\phi_0/\theta_c^2$. For small $\kappa < \kappa_0$ we then have $\gamma \approx (\kappa_0 \kappa)^{1/2}$, so we can identify $\kappa_0 = (c + c^{-1} - 2)^{1/2}$. Clearly, we need to supplement this potential with extra depth in the core region, as κ_0 for the Plummer model will not be very large for typical values of c .

One might be able to get $\gamma \propto \kappa^{1/2}$ by constructing more complicated potentials, involving an elliptical component with ellipticity growing as a function of radius (constant ellipticity does not work), or a quadrupole component of some sort. However, we can simply treat this approximation as a heuristic one, motivated by simplicity and invertability.

In order to obtain the convergence and shear from the numerical models, which are discrete in nature, we had to

apply smoothing. Even though the adaptive smoothing allows relatively high resolution to be retained in the core of the cluster, one might worry that the central values of both κ and γ are artificially reduced. Because the shear is a global function of the convergence through the convolution of eq. (2), this would be most severe for κ . We therefore tried several basic smoothing lengths, from $0.1h^{-1}\text{Mpc}$ to $0.5h^{-1}\text{Mpc}$. The ones smaller than the value of $0.25h^{-1}\text{Mpc}$ that we actually use gave the same results, i.e. similar scatter plots and the same value for c from the fit. The only difference is in the very centre of the cluster, where κ is slightly more peaked so that γ has somewhat larger maximum values. However, the discreteness of the numerical simulation does become quite visual for these small values of the basic smoothing radius. Oversmoothing affects the results more severely, pushing γ up in the outskirts and down in the centre. So, provided that the basic smoothing length is chosen sensibly, it seems that the use of adaptive window filtering results in reliable convergence, shear and magnification maps.

3.3.4 $\gamma \propto \kappa$

Another assumption which leads to a simple, invertible relation which has $\mu(0) = 1$, is $\gamma = a\kappa$. This leads to

$$\mu^{-1} = (\kappa - 1)^2 - (a\kappa)^2, \quad (28)$$

and inverts as

$$\kappa_a = 1 - \mathcal{T} \left[(1 - a^2) \mathcal{P} |\mu| + a^2 \right]^{1/2}, \quad (29)$$

where \mathcal{T} is a parity similar to the parity \mathcal{S} of the $\gamma \propto \kappa^{1/2}$ approximation. This approximation corresponds to pivoting the $\gamma = 0$ approximation around $(0, 0, 1)$ in Fig. (11). It can serve as an approximation intermediate to the $\gamma = 0$ and $\gamma = \kappa$ approximations, but it has the disadvantage of the extra parity. More importantly, this approximation is a bad fit to the numerical simulations, so we will refrain from using it.

3.4 Iterative estimate

For each of the convergence estimators discussed above, we can find an iterative solution by calculating the shear corresponding to the estimate for κ using the thin lens approximation described in Section 2.1. In other words, we use the estimate for κ to calculate the lens deflection α using eq. (2), and then get γ from α . This shear is then used to find a new estimate for κ by simply applying eq. (11). Because of the convolution, this estimate is non-local.

A problem with this estimate is that the magnification observed is usually smoothed on a scale larger than the smallest significant structures in the lens. The shear field has a strong quadrupole component, with small scale structure which is not present in the measured smoothed magnification, although it is there in the unsmoothed magnification. This means that the new estimate for κ derived from eq. (11) will have this quadrupole structure imprinted by the shear estimate. In the next step the second estimate for the shear will have even more structure on small scales, generated by the small scale structure which is present in the second estimate for κ . So convergence is not achieved.

3.5 Comparison

In principle, the best strategy, if data quality allows it, is to use the iterative method, starting from one of the estimates discussed above. If parities can be assigned reliably, κ_c seems a good choice, otherwise one should start from κ_1 , when one has only approximate knowledge about one critical line. However, because of the problems associated with the iterative estimate due to the likely smoothness of the observed lens magnification, in practice the κ_c estimator is to be preferred.

We show the caustic lines corresponding to the one-caustic and κ_c estimators for two of the lens models in Fig. (4), along with the real caustic lines for those models. Clearly the κ_c estimator has its caustic lines closest to the real ones. The one-caustic estimator is mostly useful for reference, as possible limits, of for observational data of poor quality. A comparison of caustics is not enough to compare the usefulness or goodness of the various approximations. The κ_c and κ_1 estimators, for example, cross at $\kappa = c + c^{-1} - 2$, so a total mass estimation where the total mass is calculated beyond this crossover point might be similar for both approximations. We therefore test all estimators in the next Section, both on perfect magnification data as well as on mock galaxy counts.

4 TESTING THE CONVERGENCE ESTIMATORS ON CLUSTER MODELS

We test the convergence estimators on a sample of numerical cluster models in order to examine how well each of them performs in different circumstances. The models allow us to test how well one can reconstruct the convergence from the magnification alone, by simply comparing the result of applying the estimator to the true convergence. With the addition of simple background galaxy distributions we also produce mock lensed galaxy distributions which we can 'observe', thus providing a direct test of the magnification method. Such tests should reveal intrinsic uncertainties and systematic offsets when this method is applied to observational data.

We perform two types of tests on two types of data. We test on clean simulated magnification maps with full knowledge of the image parity, and for a single source redshift, and we test on mock lensed galaxy distributions, performing the whole route from galaxy counts to mass estimation.

4.1 Estimated versus true convergence for known magnification

At this point we forget about all possible observational problems. In other words, we assume that we have a perfect magnification map of the lensing cluster (including the parity), and investigate how well the approximations allow us to reconstruct the convergence from just this magnification map. This should show us the best possible result each approximation can provide us, and reveals systematic effects associated with the estimators alone (as compared to other possible, mainly observational, sources of error).

In order to quantify these statements, we look at statistics which are based on a pixel-to-pixel comparison of estimated convergence maps to true convergence maps for a

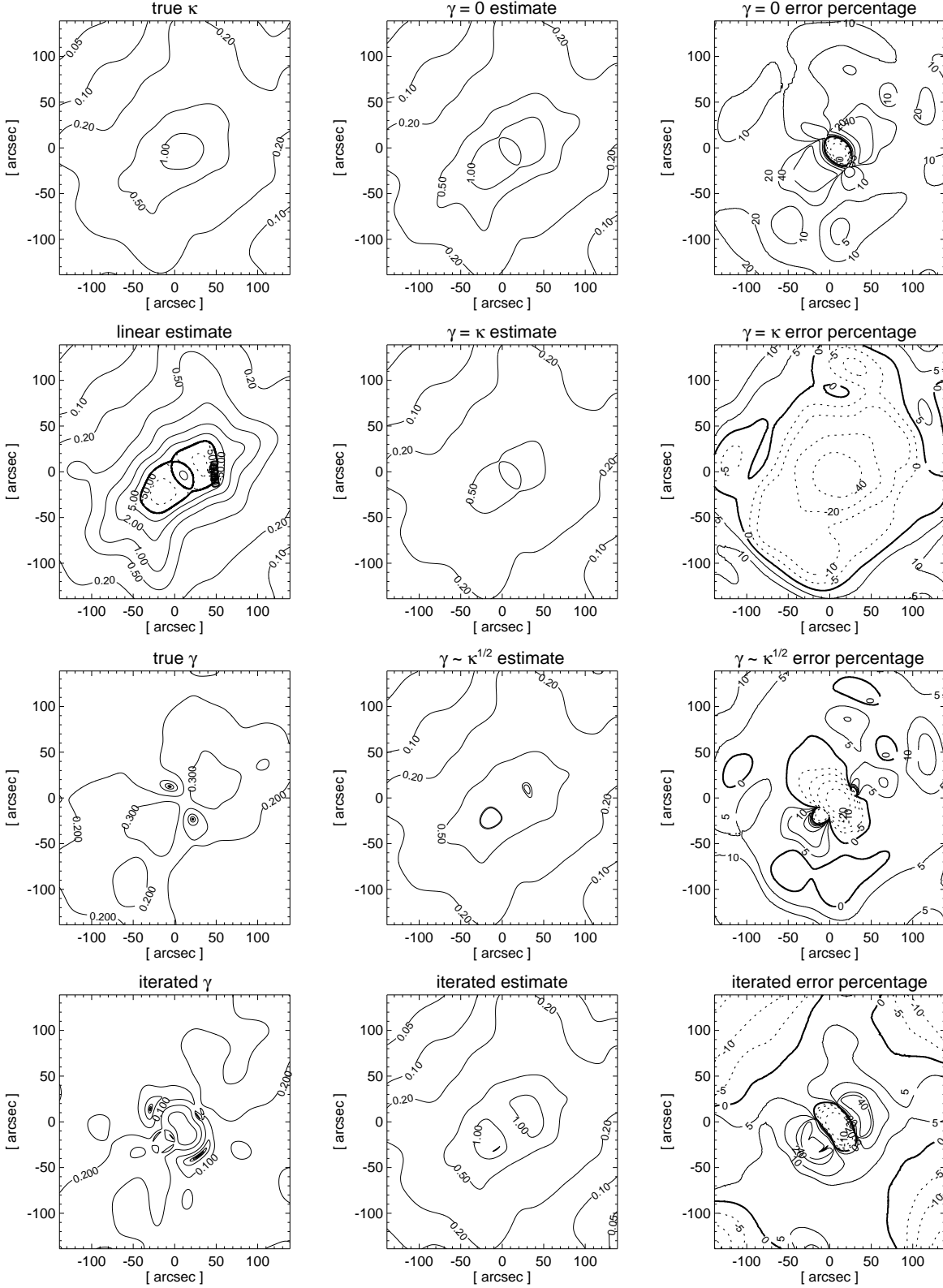


Figure 5. Comparison of estimated κ versus true κ . The middle column shows estimated κ maps for the $\gamma = 0$, $\gamma = \kappa$, $\gamma \propto \kappa^{1/2}$, and iterative (1 step) estimators. The right column shows the fractional difference (as percentages) of true versus estimated κ maps. The top left panel shows the true κ , the panel below that the linear estimate for κ , i.e. $(\mu-1)/2$. The iteratively estimated shear is shown in the bottom left corner, below the true shear. The model cluster used is the fourth entry of Table 1.

sample of rich cluster models. We are interested in the average performance for a typical rich cluster. For this purpose we selected 29 rich cluster models (see Section 3.3) from the catalogue of van Kampen & Katgert (1997). We then calculated the average of various statistics applied to each of these models. The results are listed in Table 2, and are described below.

For each model we calculated the minimum and maximum difference between the estimated and the true pixels/bins, denoted in Table 2 by ‘min’ and ‘max’ respectively, and the average over all pixels of this difference, denoted by ‘mean’. These statistics describe local and mean deviations from the true convergence. Two more statistics describe the scatter in the residual of true minus estimated convergence: ‘abs’ is just the average absolute deviation, while ‘rms’ is the standard *r.m.s.* deviation. These are good measures for the accuracy of the estimators. All statistics were calculated for absolute differences in κ , and for fractional differences, expressed in percentages.

An additional estimator has been added to Table 2, labeled ‘mean’, which just comprises taking the mean of the $\gamma = 0$ and $\gamma = \kappa$ estimators. This estimator has no physical basis, and even produces imaginary shear for some values of κ , but might be useful in practice as the $\gamma = 0$ estimator tends to overestimate and the $\gamma = \kappa$ tends to underestimate.

4.1.1 Maps

Using the thin lens approximation, as summarized in Section 2.1, we produce maps of the lens convergence, shear and magnification for the selected four cluster models. We then use the magnification only (with full knowledge of its parity, though), to reconstruct convergence maps using the various assumptions about the shear, and compare these to the true convergence. This is shown in Fig. 5 for the most massive model cluster, as this one has the largest range of possible κ values and therefore provides the most stringent tests for the estimators. Note that this cluster has a value of σ_8 which is far larger than allowed for the standard CDM scenario (e.g. van Kampen & Katgert 1997 and references therein).

In Fig. 5 we see that linear estimator performs very poorly, as it just follows the magnification, including the caustics. It is only doing well for small κ , as expected. The $\gamma = 0$ assumption produces an overestimate for the convergence for all regions of the cluster. The $\kappa = \gamma$ estimator underestimates the mass in the central regions of the cluster, and (slightly) overestimates for $\kappa < 0.2$. The $\gamma \propto \kappa^{1/2}$ estimator clearly performs best, even better than the iterative estimator.

As the cluster shown in Fig. 5 is fairly extreme, we should consider the performance statistics listed in Table 2 that were obtained for the rich cluster sample, which contains less evolved clusters with smaller overall convergences. Much of what was seen in Fig. 5 is now expressed quantitatively. The linear estimator diverges, while the $\gamma = 0$ and $\gamma = \kappa$ estimates generally over- and underestimate, respectively. Note that the fractional and absolute statistics weight pixels differently, the former giving more weight to the more noisy pixels outside of the cluster, and the latter to the central regions. This results in a mean overestimate in the fractional statistics of both the $\gamma = 0$ and $\gamma = \kappa$ estimators. The $\gamma \propto \kappa^{1/2}$ and iterative estimators perform

best, although the improvement over the other estimators is certainly not dramatic.

4.1.2 Radial profiles

Besides testing the estimators on the full 2D map of the lens magnification, which is hard to obtain in practice, we test them on azimuthally averaged ‘magnification profiles’ as well. These have already been obtained observationally (Fort et al. 1997; Taylor et al. 1998), and are therefore of particular interest.

Again we first look at radial binning of the magnification map directly obtained from a numerical simulation, i.e. we only investigate the effect of the annular binning procedure. We performed the same statistics on the same model cluster sample as above, but now on the radially binned data. One expects that the binning reduces the scatter in the local relations, but at the same time binning means loss of information, especially for clumpy aspherical clusters.

From the performance statistics listed in the lower half of Table 2 we can see that the performance for profiles is worse than for the maps. This stems from the fact that a lot more weight is put on the central region of the clusters due to the annular binning, where the uncertainties are largest. The $\gamma = 0$ and $\gamma \propto \kappa^{1/2}$ approximations clearly perform best in terms of accuracy, as expressed by the *r.m.s.* statistic, whereas the mean of the $\gamma = 0$ and $\gamma = \kappa$ estimator has the smallest systematic error.

4.2 Estimated versus true convergence for simulated observational data

4.2.1 Simulated background galaxy distributions

The tests we performed so far were for the best possible data set, a continuous magnification map or annular profile, with known sign, and one source redshift. Obviously, this is not going to be the case for observational data, which has many intrinsic uncertainties as described in Section 2.3.

The main intrinsic source of error is the clustering of background galaxies, the variation in their redshifts, and the fact that we usually have a limited number of galaxies to count, which introduces shot noise. In order to examine the effect of these uncertainties on the convergence estimate, we need to construct magnification maps derived from number counts of a clustered set of background galaxies which are at different redshifts.

We use background galaxy distributions which were generated as in BTP, who adopt the lognormal-Poisson model (Coles and Jones 1991) as a simple but sufficient model for the clustering of background galaxies. These galaxies were generated in planes of constant redshift, with luminosities drawn from a Schechter luminosity function

$$\phi(L) = \phi_*(z) \exp(-L/L_*), \quad (30)$$

where $\phi_*(z) = 0.02h^2(1+z)^2 \text{Mpc}^{-3}$, and L_* is taken constant. The redshift distribution for these galaxies can be well approximated by $n(z) = 4z_*^{-3}z^2e^{-2z/z_*}$, with $z_* = 0.8$. Like BTP, we consider R band counts. In order to be able to count lensed (i.e. amplified!) distributions down to a limiting magnitude m_{lim} , we generate background distributions down to at least $m_{\text{lim}} + 1$.

Table 2. Performance statistics of the convergence estimators, based on a pixel-by-pixel comparison of the estimated versus true convergence maps (top half), and a bin-to-bin comparison for the estimated versus true profiles. A positive sign corresponds to overestimating the convergence. Please refer to the main text for a description of the statistics.

| Statistic | linear | $\gamma = 0$ | $\gamma = \kappa$ | mean | $\gamma \propto \kappa^{\frac{1}{2}}$ | Iterat. |
|---|---------|--------------|-------------------|-------|---------------------------------------|---------|
| Absolute statistics for 2D maps | | | | | | |
| min | -0.01 | -0.09 | -1.19 | -0.57 | -0.43 | -0.12 |
| max | 7.27 | 0.23 | 0.06 | 0.10 | 0.06 | 0.11 |
| mean | 0.11 | 0.01 | -0.02 | -0.01 | -0.02 | -0.01 |
| abs | 0.11 | 0.01 | 0.03 | 0.02 | 0.03 | 0.01 |
| rms | 0.46 | 0.03 | 0.09 | 0.04 | 0.04 | 0.01 |
| Fractional statistics for 2D maps | | | | | | |
| min | -6.04 | -6.09 | -6.50 | -6.13 | -6.93 | -8.32 |
| max | 21.53 | 1.97 | 1.37 | 1.64 | 0.75 | 0.70 |
| mean | 0.68 | -0.49 | -0.83 | -0.66 | -1.58 | -1.44 |
| abs | 1.87 | 0.97 | 1.04 | 0.96 | 1.61 | 1.47 |
| rms | 2.72 | 1.24 | 1.17 | 1.18 | 1.18 | 1.52 |
| Absolute statistics for radial profiles | | | | | | |
| min | 0.05 | -0.20 | -6.44 | -2.74 | -1.78 | – |
| max | 864.70 | 1.78 | 0.11 | 0.26 | 0.12 | – |
| mean | 20.02 | 0.33 | -0.72 | -0.19 | -0.32 | – |
| abs | 20.02 | 0.35 | 0.78 | 0.34 | 0.34 | – |
| rms | 86.38 | 0.44 | 1.65 | 0.69 | 0.44 | – |
| Fractional statistics for radial profiles | | | | | | |
| min | 2.40 | 0.06 | -11.35 | -4.79 | -4.97 | – |
| max | 1121.60 | 4.60 | 1.80 | 2.74 | -0.92 | – |
| mean | 37.61 | 2.26 | -1.39 | 0.44 | -2.90 | – |
| abs | 37.61 | 2.35 | 2.68 | 1.79 | 3.01 | – |
| rms | 116.44 | 1.23 | 3.73 | 2.02 | 1.11 | – |

The field count slopes of these distributions for two magnitude intervals and two lens redshifts are obtained from fits to the luminosity functions of the 32 samples generated. This is shown in Fig. 7, with the values of the slopes annotated. These luminosity functions are good fits to the observed ones (e.g. Metcalfe et al. 1995), except possibly for the faint end, where the slope should remain roughly constant instead of flattening down, i.e. where the simple assumptions of BTP are likely to break down. However, the observations at the faint end are still contradictory. Furthermore, a flattening slope actually provides a useful test for our methods, as other bands like the U-band will show this behaviour.

With these background distributions it is straightforward to produce mock observations. All galaxies (i.e. down to $R = 25$) are mapped to the image plane using the lens mapping, with the deflection angle calculated using the thin lens approximation, as described earlier. We then select galaxies for counting from a range in magnitude.

Before we can obtain a magnification map from these number counts, we need to either smooth the number count distribution, or azimuthally bin the counts to obtain count

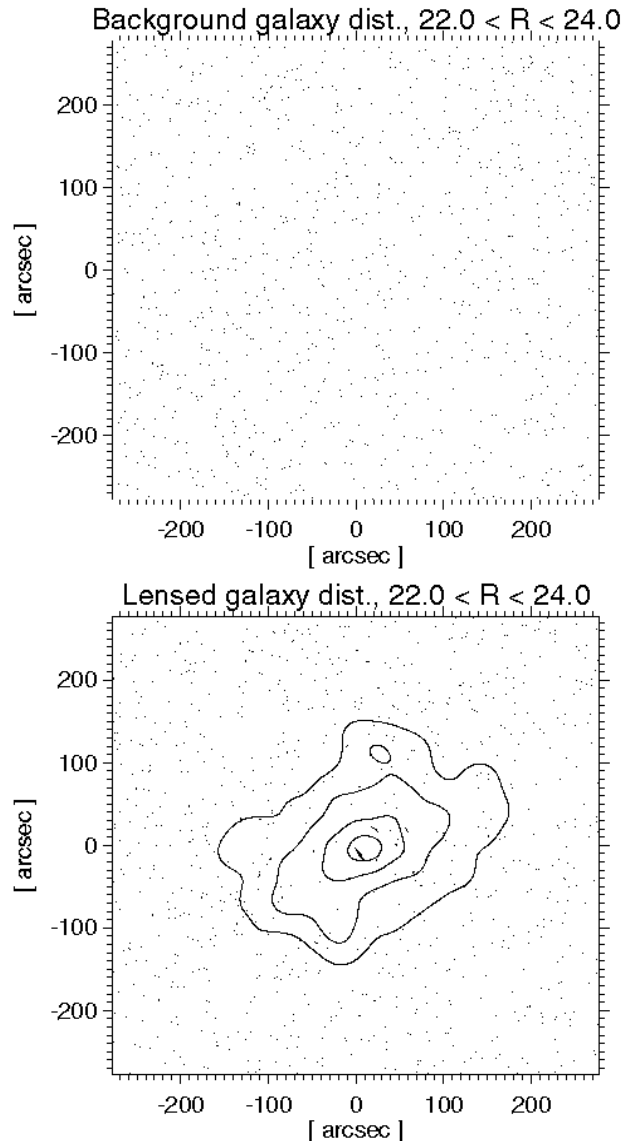


Figure 6. Example of a number count simulation. The top panel shows a generated background galaxy distribution using the simple model of BTP. The bottom panel shows the same distribution lensed, with the true convergence contours superimposed (for $z_s = 0.8$). Galaxies are generated up to $R = 25$, but only plotted in the range $22 < R < 24$. This allows for a factor of 2.51 magnification, which is sufficient in most cases.

profiles. For a limited number of galaxies this is the only feasible alternative. We consider both alternatives, and test for the intervals $22 < R < 24$. An example of the former is given in Fig. 6, which shows a background distribution cut to $22 < R < 24$ and its corresponding lensed distribution, also cut to $22 < R < 24$ but obtained using the full $R < 25$ background population. Close to the caustics the amplification will be more than one magnitude (i.e. $\mu > 2.51$), so we are likely to miss a few galaxies there, which will slightly enhance the presence of the caustics in our simulations.

The mock observations do not simulate colour cutting, and problems associated with masking the cluster galaxies. The cluster galaxies are modelled (see van Kampen & Katgert 1997 for details), and take part in the lensing, but are

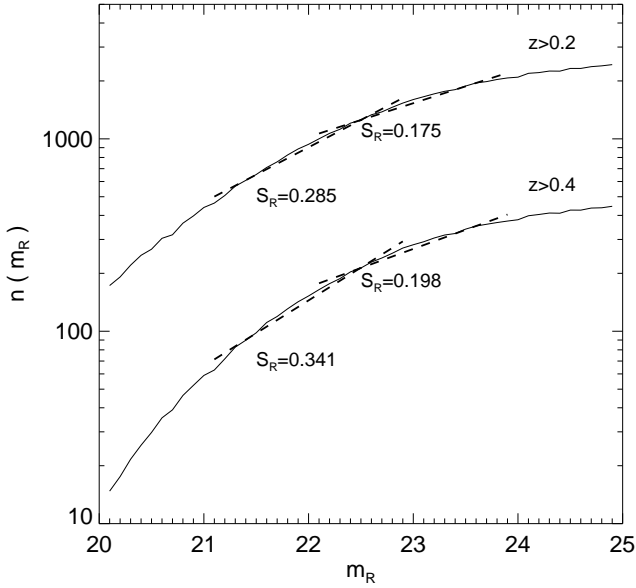


Figure 7. Cumulative luminosity function for all 32 backgrounds stacked together, with fits for the average slope over a range in R . The top curve is for galaxies beyond $z = 0.4$, the bottom one for $z > 0.2$. The normalisation is arbitrary, and chosen for clarity.

not put in the observed image and then masked out. These observational difficulties are hard to model, and beyond the scope of the present paper.

4.2.2 Setting parity and the estimator parameters

Setting the parity is the biggest problem for all estimators, and will be the most significant uncertainty in the central regions of the observed cluster. However, giant arcs, especially with redshifts measured, can be used to guess where the caustics are. In the tests we performed above the parity was determined from the simulations, i.e. we actually used the sign of μ for estimating the convergence. We now disregard any such knowledge, and set the parity by hand.

Concerning the $\kappa \propto \gamma^{1/2}$ approximation, we can get its parameter c from observed data only if we make an assumption for the behaviour of κ between the critical curves. For number counts in radial bins we can estimate c if we know both the position of the minimum μ_{\min} , θ_{\min} , and one of the critical lines (or both), θ_{inner} or θ_{outer} , and assume a functional form for κ as a function of θ within the range $[\theta_{\text{inner}}, \theta_{\text{outer}}]$. For example, the assumption that between the critical lines $\kappa \propto \theta^{-1}$ leads to:

$$c \approx \left(2 \frac{\theta_{\text{outer}}}{\theta_{\min}} - 1\right)^{\frac{1}{2}} \approx \left(2 \frac{\theta_{\text{inner}}}{\theta_{\min}} - 1\right)^{-\frac{1}{2}} \approx \left(\frac{\theta_{\text{outer}}}{\theta_{\text{inner}}}\right)^{\frac{1}{2}}. \quad (31)$$

If all three characteristic positions are measurable, an average of the three c -estimators should provide the best estimate. We can use this estimate for c to estimate $\kappa(\theta)$, and use that to obtain a new estimate for c . Such an iteration should work if we deal with the parities properly.

4.2.3 Smoothed maps from discrete number counts

We generate mock number counts by lensing background distributions which were produced up to the red magnitude

$R = 25$ as described in Section 4.1.1. We then count galaxies in the range $22 < R < 24$ only. For almost all galaxies the magnification is less than one magnitude, so this provides a good approximation. We also count galaxies in the same field-of-view for the unlensed distribution, in order to obtain the field count N_0 . The average slope S_R is fitted from a reconstructed luminosity function obtained from the same unlensed distribution, as this depends on the redshift of the lens, z_D . For several z_D 's and R ranges we show these fits for S_R in Fig. 7.

In the case that we have a sufficient number of background galaxies we can try to obtain a magnification map from the number counts. We have to deal with shot noise, and therefore obtain a smoothed number count map from the discrete galaxy distribution. This is *not* straightforward, as we have to deal with caustics, where $\mu^{-1} = 0$. If we smooth the number counts without taking parity into account, there will be few points on the map that even approach zero after the smoothing operation. We therefore apply the following ‘trick’: we already set parity by setting N/N_0 negative where we believe that μ^{-1} is negative. This ascertains that the caustics we fix by setting the parity remain in place, and gives a much better estimate for the magnification near the caustics as well.

The smoothing scale needed is determined by the average surface number density of galaxies. We set it to be three times the Poissonian nearest neighbour distance, i.e. $3(\pi \langle n \rangle)^{-1/2} \approx 1.7 \langle n \rangle^{-1/2}$. This is to make sure the smoothing is sufficient for the core region, which is relatively devoid of galaxies due to the effect we try to measure.

An example of estimating the convergence map from simulated number counts is shown in Fig. 8. Again the fourth cluster from Table 1 was used. As it is put at a redshift of 0.4, we used a slope $S_R = 0.197$ for obtaining the magnification map from the number counts. We see that we can reasonably well reconstruct the *main features* of the convergence map from these counts, but a lot of information is lost. The cluster is detected, most precisely by the $\gamma \propto \kappa^{1/2}$ estimator, but the limitations of the magnification method are obvious. Of course one can simply improve signal-to-noise by going to fainter magnitudes, which increases the number of galaxies and includes galaxies at higher redshift, which pushes up the convergence.

4.2.4 Annular binning of number counts

Usually the number of background galaxies is not sufficient to produce 2D magnification maps, and one is restricted to counts in annular bins. We again only select galaxies with R magnitudes in the range $22 < R < 24$, and count them in bins around the centre found from the galaxy distribution (the cluster models contain galaxies as well, see van Kampen & Katgert 1997). Proceeding from number counts to magnification and convergence estimates as before, we now obtain estimated convergence profiles. We do this for 32 different backgrounds, in order to get an estimate for the intrinsic error on the number counts due to shot noise and background clustering.

This procedure is illustrated in the top panel of Fig. 9, where we show the number count profile for one background (thick solid line), with intrinsic error bars, obtained using all backgrounds, superimposed. The thin solid line that is also

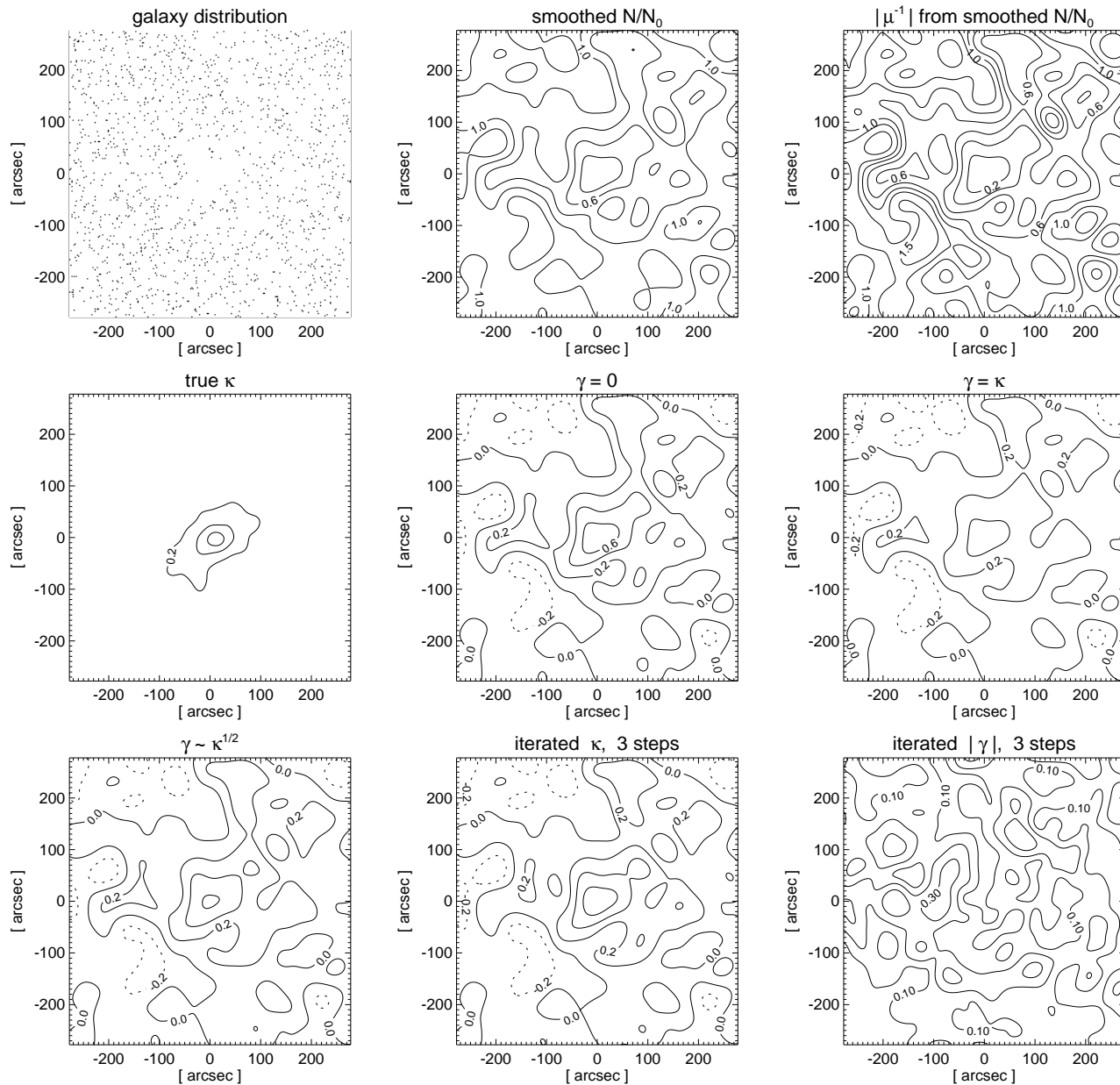


Figure 8. Illustration of the complete route from number counts to estimation of the lens convergence, for a fairly massive cluster (the fourth entry from Table 1). The top left shows the number count distribution in the range $22 < R < 24$, which is smoothed as described in the main text to obtain a map of number count variations, N/N_0 . From this map we obtain the magnification map, shown in the top right panel. The fourth panel shows the true convergence map, obtained directly from the numerical simulation, which we try to estimate. The next four panels show estimates obtained from the magnification map alone, for, respectively, the $\gamma = 0$ approximation, for $\gamma = \kappa$, for $\gamma \propto \kappa^{1/2}$, and performing three steps of the iterative scheme. The bottom right panel shows the shear corresponding to this iterative estimate.

plotted shows the average over 32 different number count profiles obtained by just changing the background population. The middle panel of Fig. 9 shows the reconstruction of the convergence profile for the single background, along with the convergence profile obtained directly from the simulation. The bottom panel shows the same, but now for the averaged profile. The reconstruction for the latter is obviously better. But despite the noise, one can clearly get a fair estimate for the convergence profile from number counts alone.

Finally, we examine how well we can estimate the total mass within a certain annulus from these count simulations. We simply convert convergence to surface mass density using the mean redshift of our background galaxies, which is around 0.8 for the simulations shown, and integrate that to obtain a projected mass within $0.5h^{-1}\text{Mpc}$. We then compare this mass estimate for the cluster to the mass obtained directly from the numerical cluster model.

Fig. 10 shows the results of this exercise. The top panel shows the distribution over estimated masses for the sam-

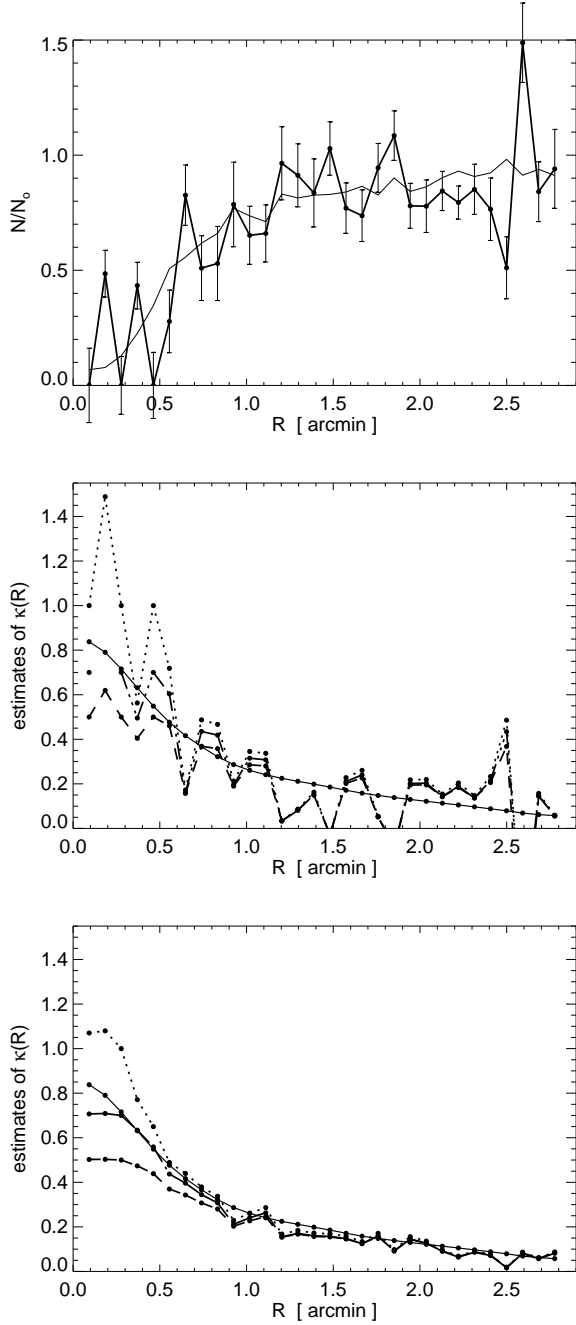


Figure 9. Simulated number count profiles for the same cluster used for Fig. 8, and also for $22 < R < 24$. The top panel shows a number count profile for a single profile (thick solid line), along with the average of number count profiles for 32 different profiles (thin solid line). The latter provide an estimate for the intrinsic uncertainty due to shot noise and clustering of the background galaxies, and these are overplotted as error bars. The second panel shows the convergence estimates from the single background number count profile shown in the top panel, for $\gamma = 0$ (dotted line), $\gamma = \kappa$ (dashed line), and $\gamma \propto \kappa^{1/2}$ (dot-dash line). The true convergence profile, for $z_s = 0.8$, is plotted as a solid line. The bottom panel shows the same, but for the average over 32 different background populations. A intrinsic count slope of 0.198 is used.

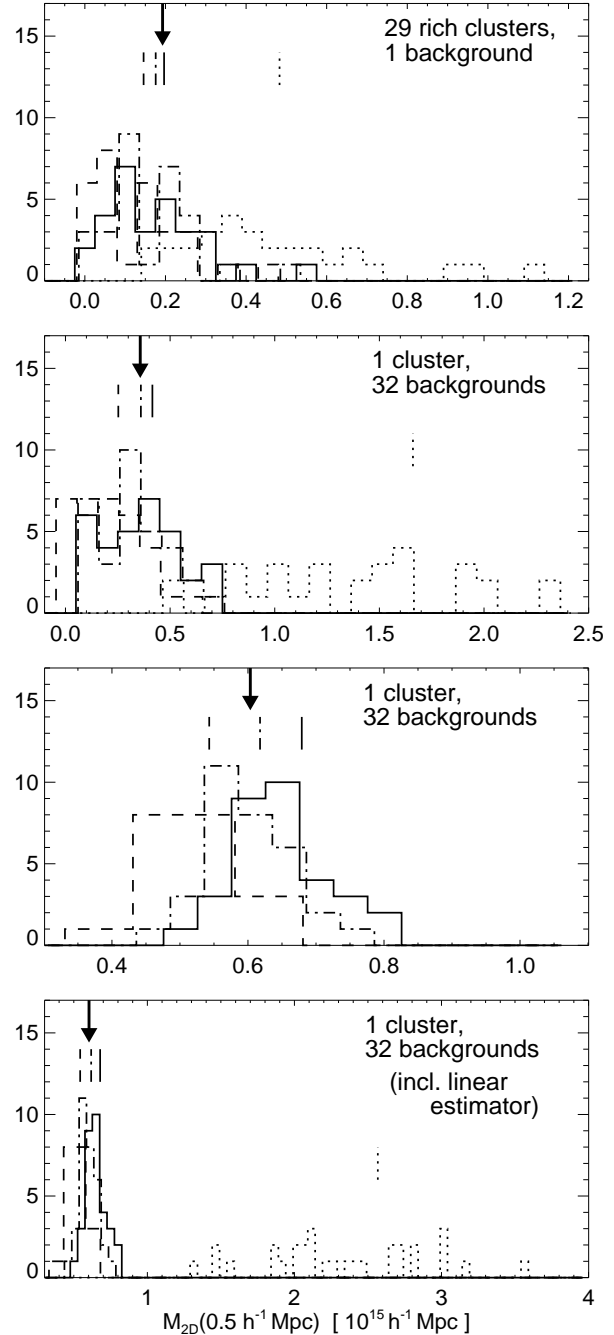


Figure 10. Histograms of estimated total projected cluster masses within $0.5 h^{-1} \text{Mpc}$, obtained from number count profiles. Dotted lines denote the linear (weak lensing) approximation, solid lines are for $\gamma = 0$, dashed for $\gamma = \kappa$, and dot-dashed for $\gamma \propto \kappa^{1/2}$. The top panel shows the distribution for 29 rich clusters put at $z_D = 0.4$ in front of the same background galaxy population. The vertical lines indicate the average over the estimated projected masses of these clusters, while the arrow show the average over their true projected masses. The second panel shows the same, but now for one cluster (entry three from Table 1) in front of 32 different backgrounds. The lines and arrow are now the estimated and true masses of that cluster. The third panel shows the same cluster for larger σ_8 , i.e. more massive. The fourth panel is the same as the third, but with the linear estimator included.

ple of rich clusters that we considered before. The arrow indicates the mean *true* mass for this sample, whereas the vertical lines give the mean for the estimated masses. The linear mass estimate is a factor of two too large, while all other estimators give similar values, with the $\gamma = 0$ estimator performing marginally better. Just one background was used, but we can also consider the effect of changing the background, i.e. cosmic variance, by putting a single cluster in front of 32 different backgrounds. This is shown in the second panel of Fig. 10, for the third cluster from Table 1. As this cluster is one of the most massive from the sample, it is no surprise to see that the linear estimator is now on average a factor of four too large, with a huge scatter. The other estimators have a significant scatter as well, quantifying what was already seen in Fig. 8. This scatter decreases for larger convergences, when looking at the same cluster for larger σ_8 (shown in the third panel). The cluster is then more evolved and therefore more massive. The last panel is the same as the third, but with the linear estimator included, which is now quite far off. We see that for the more massive clusters the $\gamma \propto \kappa^{1/2}$ estimator works best *on average*, but that the scatter among the estimators is quite similar.

5 OBSERVED CLUSTERS

We apply the non-linear estimators for the lens convergence to published observational data, in order to test whether reasonable mass estimates for real clusters can be made, and how these compare to masses determined using other, independent techniques. We also like to establish what the errors are due to the uncertainty in the assumptions of the non-linear estimators when applied to real data, especially for the heuristic estimator. After all, so far we only tested the heuristic estimator on cluster models which were also used to find that estimator. Presently, data of sufficient quality exists for two clusters only, CL 0024+1654 and A1689.

5.1 CL 0024+1654

Fort, Mellier & Dantel-Fort (1997) have published number counts in radial bins for this $z = 0.39$ cluster, in both the *I*-band and the *B*-band. They present counts as surface density profiles, and also provide the field number counts (which we denote by N_0). For the *I*-band they only count galaxies in the magnitude range $25 < I < 26.5$, for the *B*-band in the range $26 < B < 28$. The main reason for this is completeness, but also the fact that they find a field luminosity function with a fairly constant slope for these intervals: $S_I = 0.25 \pm 0.03$ and $S_B = 0.17 \pm 0.02$ respectively. These values correspond to $\beta_I = -2.67$ and $\beta_B = -1.74$. Furthermore, a giant arc is observed at 37 arcsec, but its redshift is unfortunately unknown. However, Fort et al. (*ibid.*) argue that it should be close to the mean for the background population, so we can use its position to set the parity for our estimators.

The relative number counts N/N_0 in *I* and *B* are plotted in Fig. 11(left panels), along with the various estimators for the convergence κ (middle panels). Parity was assigned according to the position of the arc, indicated by a short vertical line in the figure. The number counts were smoothed with the parities applied, as described in Section 4.2. This

smoothing is really necessary, as the galaxy number density is fairly small: 6.13 arcmin^{-2} for the *B*-band, 3.32 arcmin^{-2} for the *I*-band, which is even smaller than for the simulation example shown in Fig. 6. The number of bins used by Fort et al. (*ibid.*) is too large, given these densities. The smoothing length that corresponds to these number densities is about 40 arcsec and one arcmin respectively if one would try to construct a number count map (see Section 4.2.3). For profiles, the smoothing length necessary is a decreasing function of radius. However, the number density of galaxies is increasing with radius (due to the magnification effect). It is therefore reasonable to use a constant smoothing length for the profiles. We have adopted 20 arcsec for the *B*-band, and 30 arcsec for the *I*-band.

The *B*-band data pose a problem for the $\gamma \propto \kappa^{1/2}$ estimator, as the counts rise all the way back to N_0 at about 10 arcsec. We therefore switch to the ‘mean’ estimator, described in Section 4.1, at the position where the $\gamma \propto \kappa^{1/2}$ estimator becomes undefined. This switch is indicated by a diamond symbol in the bottom central panel. This procedure is unsatisfactory, of course, but it seems the best possible alternative for this particular dataset, which is not of high-quality anyway.

From the convergence profiles we calculate projected mass profiles, assuming that all background galaxies are at $z_s = 1$. These are plotted in the right hand side panels of Fig. 11, where the angular scale is transformed to a physical scale, assuming that $\Omega_0 = 1$. We find that the masses estimated from the *B*- and *I*-bands are roughly consistent with each other: for both bands we obtain a total projected mass within $0.3h^{-1}\text{Mpc}$ of approximately $0.7 - 0.8 \times 10^{15} h^{-1} M_\odot$ using the heuristic estimator. If we treat the $\gamma = 0$ and $\gamma = \kappa$ estimators as upper and lower limits respectively, which in general is not correct, we have an uncertainty of $0.2 \times 10^{15} h^{-1} M_\odot$ due to the uncertainty in the choice of estimator.

Kassiola, Kovner & Fort (1992) published a mass model for this cluster that was fitted to various lensing features. They quote a total mass of about $10^{14} h^{-1} M_\odot$ within $0.1h^{-1}\text{Mpc}$. Our isothermal estimator gives roughly the same mass within that radius, in both bands. It also gives a mass of $1.6 \times 10^{15} h^{-1} M_\odot$ within $0.5h^{-1}\text{Mpc}$, which we should consider a lower limit as the isothermal estimator typically underestimates masses.

Bonnet, Mellier & Fort (1994) have measured the tangential shear profile for this cluster, and estimated the mass within $1.5h^{-1}\text{Mpc}$ to be $1 - 2 \times 10^{15} h^{-1} M_\odot$, depending on the assumption for the density profile. This range contains the mass we find within a radius of $0.5h^{-1}\text{Mpc}$, so in order to be consistent, we need to assume that the mass within $1.5h^{-1}\text{Mpc}$ is close to the upper limit given by Bonnet et al. (*ibid.*), or that most of the cluster mass resides in the inner $0.5h^{-1}\text{Mpc}$.

However, looking at the counts (left hand panels of Fig. 11), we see that the counts never reach the N_0 given by Fort et al. (1997). This is not too important for the central regions of the cluster, where the counts are low anyway, but in the outskirts it yields a significant contribution to the total mass. If we take a value of N_0 to which the counts do converge, which is 20 per cent smaller than the one taken from Fort et al. (*ibid.*), we find that the mass within $0.5h^{-1}\text{Mpc}$ is about $1.0 \times 10^{15} h^{-1} M_\odot$, while the mass within $0.1h^{-1}\text{Mpc}$

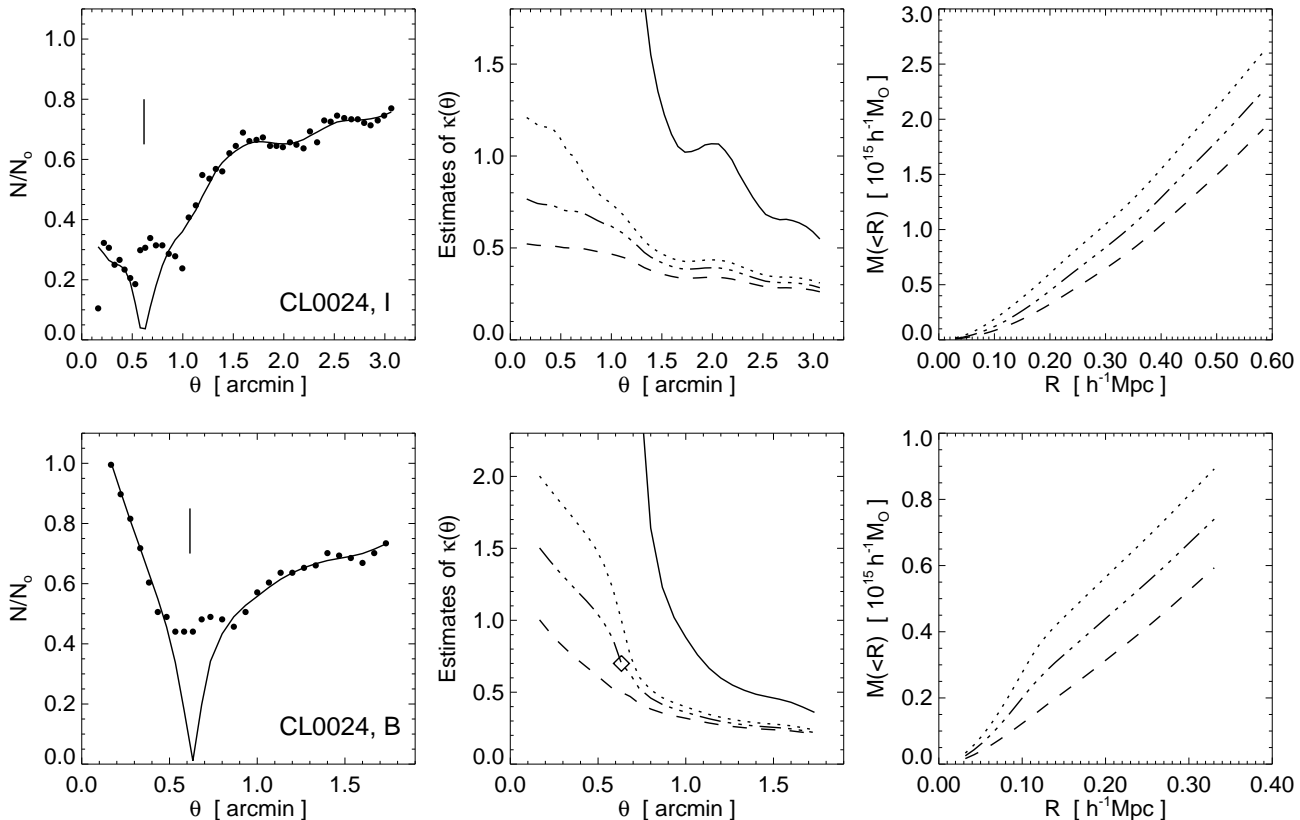


Figure 11. Convergence estimates for the clusters CL0024, in the *I* and *B* band. The left hand panels show the number count profile, where the dots represent the binned number counts published by Fort et al. (1996) and the solid lines the smoothed number counts with parity taken into account (see text for details). The middle panels show the convergence estimates for the various assumptions made: weak lensing (solid line), $\gamma = 0$ (dotted line), $\gamma = \kappa$ (dashed line), $\gamma \propto \kappa^{1/2}$ (dot-dash line). The same linetypes have been used to plot the corresponding cumulative mass profiles in the right hand panel. The position of a giant arc is indicated by a vertical line. The diamond symbol indicates a switch in estimators, explained in more detail in the main text.

does not change much. This seems a more consistent mass estimate for CL 0024+1654 from the lens magnification. It is therefore essential to get a better observational determination for the field count N_0 .

Fort et al. (*ibid.*) also published preliminary data on A370, but we believe these not to be of sufficient quality to attempt mass estimation, especially since the position of the minimum in the number counts is far removed from the position of a giant arc observed in this cluster (Soucail et al. 1988).

5.2 A1689

We summarize the results for A1689, as published by Taylor et al. (1998). The total mass within $0.24h^{-1}\text{Mpc}$ was found to be $0.5 \pm 0.09 \times 10^{15} h^{-1} M_{\odot}$, in fair agreement with X-ray, virial, and weak shear mass estimates. The number of background galaxies used was roughly similar to that used in the count simulations presented in Section 4.2, and the uncertainties are therefore quite similar, i.e. on the order of 50 per cent. A1689 has a giant arc, but just like for CL 0024+1654, the redshift of this arc is unknown, which leaves an ambiguity in the interpretation. Note that the total exposure time used to take the A1689 data was quite short (less than 3

hours in the *V* and *I* bands), so an improvement on this is easily achieved.

6 CONCLUSIONS AND DISCUSSION

In order to be able to estimate the lens convergence κ from the lens magnification μ , we searched for a realistic approximation between either of these quantities and the lens shear γ , which needs to be taken into account in the strong lensing regime. We looked at simple analytical lens models with exact relations between the three lens quantities, notably the $\gamma = 0$ approximation, corresponding to a uniform sheet of matter, and the isothermal model, which has $\kappa = \gamma$.

As these do not provide adequate descriptions for neither observed nor simulated clusters, we have studied the lensing properties of a complete catalogue of galaxy cluster models to find an approximation for the shear which still allows a simple inversion from magnification to convergence. A approximation that does just that is $\gamma \propto \kappa^{1/2}$, which leads to a simple two-caustic magnification-convergence relation. A disadvantage of this approximation is that two parities have to be set, which can be a problem for observational data, as the sign of the magnification cannot be directly measured.

We also discussed the iterative technique, where one starts with any of the estimators mentioned to obtain an estimate for the shear using the thin lens approximation, and then uses that shear to calculate a new convergence estimate. However, this method is not likely to converge for observational data because the dominant quadrupole structure of the shear field will not be present in the observed magnification field, which usually needs to be smoothed fairly heavily. The iterative estimate is still useful, however, if one performs a few steps only, or preferably just one.

Two types of tests were performed on all estimators considered: the ideal case for which full knowledge of the magnification distribution exists (including its sign), and the case where we start from mock lensed background galaxy counts, mimicking intrinsic problems like the clustering of these galaxies and shot noise due their limited number.

The first type of tests have shown that if the magnification is perfectly known, the mass distribution of these cluster models can be fairly well reconstructed using the estimator based on a the relation and convergence of the form $\gamma \propto \sqrt{\kappa}$, or the iterative estimator operated for one step only. The isothermal estimate generally underestimates the surface mass density for $\kappa > 0.3$, and overestimates for smaller κ . The $\gamma = 0$ estimator overestimates for all κ up to the first caustic, and can therefore be considered a strict lower limit for these κ .

The second type of tests aimed at mimicking observational data, i.e. going from number counts to convergence estimates. We showed that it is still possible to reconstruct the convergence for simulated clusters, although the intrinsic uncertainties become significant. We have also demonstrated that the mass estimated using the weak lensing approximation is at least twice the real mass, thus showing that one really needs to go beyond the weak lensing approximation to get sensible cluster mass estimates.

We used published number counts for the cluster CL 0024+1654 (Fort et al. 1997) to illustrate the non-linear mass estimation technique. We showed that the total mass estimated compares fairly well to estimates from other techniques, even though the quality of the data is relatively poor. The uncertainties in the mass found for both this cluster and for A1689 (Taylor et al. 1997) are quite large still, but there are many ways to reduce these. We can get (photometric) redshifts for the background galaxies, find a better value for the field number count, obtain the redshifts of the arcs, and use wavelengths for which the luminosity function is either much steeper or much shallower than the slope of 0.4 for which there is no variation in number counts at all. Also, we should go to fainter magnitudes, in order to get higher background galaxy number densities, which minimizes the clustering and shot noise problems. Furthermore, the lens becomes stronger as the convergence gets larger due to the higher mean background galaxy redshift.

In concluding, we showed that mass estimation from lens magnification in the strong lensing regime is possible. We seem to find consistent mass estimates for both CL 0024+1654 and A1689 with only limited observational data available. This should give us encouragement to obtain better data for these and other clusters. Obviously, in combination with other mass estimates the lens magnification technique will be even more promising.

ACKNOWLEDGMENTS

The author thanks Andy Taylor for supplying the mock background galaxy distributions and for useful discussion and comments, John Peacock, Alan Heavens, Jens Hjorth, Cedric Lacey and Frank Pijpers for useful discussion and comments, and acknowledges an European Community HCM Research Fellowship for financial support. This work was supported in part by Danmarks Grundforskningsfond through its funding of the Theoretical Astrophysics Center.

REFERENCES

- Bartelmann M., Weiss A., 1994, *A&A*, 287, 1
 Bartelmann M., 1995, *A&A*, 303, 643
 Bartelmann M., Steinmetz M., Weiss A., 1995, *A&A*, 297, 1
 Bartelmann M., Narayan R., Seitz S., Schneider P., 1996, *ApJ*, 464, L115
 Broadhurst T.J., Taylor A.N., Peacock J.A., 1995, *ApJ*, 438, 49
 Bonnet H., Mellier Y., Fort B., 1994, *ApJ*, 427, L83
 Coles P., Jones B.J.T., 1991, *MNRAS*, 248, 1
 Fort B., Mellier Y., 1994, *A&AR*, 5, 239
 Fort B., Mellier Y., Dantel-Fort M., 1997, *A&A*, 321, 353
 Gorenstein M.V., Falco E.E., Shapiro I.I., 1988, *ApJ*, 327, 693
 van Kampen E., 1994, PhD Thesis, Rijksuniversiteit Leiden
 van Kampen E., 1996, in Martínez, V.J., Coles, P., eds., Mapping, Measuring, and Modelling the Universe, ASP Conference Series Vol. 94, p. 265
 van Kampen E., 1997, in Clarke D.A., West M.J., eds., Computational Astrophysics, ASP Conference Series Vol. 123, p. 231
 van Kampen E., Katgert P., 1997, *MNRAS*, 289, 327
 van Kampen E., 1998, in preparation
 Kaiser N., 1995, *ApJ*, 493, L1
 Kaiser N., 1996, in Lahav O., Terlevich E., Terlevich R.J., eds., 'Gravitational Dynamics', Proc. of the 36th Herstmonceux Conference. Cambridge Univ. Press, Cambridge, p. 181
 Kaiser N., Squires G., 1993, *ApJ*, 404, 441
 Kassiola A., Kovner I., Fort B., 1992, *ApJ*, 400, 41
 Katgert P., Mazure A., Jones B., den Hartog R., Biviano A., Dubath P., Escalera E., Focardi P., Gerbal D., Giuricin G., Le Fèvre O., Moles O., Perea J., Rhee G., 1995, *A&A*, 310, 8
 Kochanek C.S., Blandford R.D., 1991, *ApJ*, 375, 492
 Mazure A., Katgert P., den Hartog R., Biviano A., Dubath P., Escalera E., Focardi P., Gerbal D., Giuricin G., Jones B., Le Fèvre O., Moles O., Perea J., Rhee G., 1995, *A&A*, 310, 31
 Metcalfe N., Shanks T., Fong R., Roche N., 1995, *MNRAS*, 273, 257
 Schneider P., 1995, *A&A*, 302, 639
 Schneider P., Ehlers J., Falco E.E., 1992, *Gravitational Lenses*, Berlin: Springer
 Schneider P., Seitz C., 1995, *A&A*, 297, 411
 Silverman B., 1986, *Density Estimation for Statistics and Data Analysis*, London: Chapman and Hall
 Soucail G., Mellier Y., Fort B., Mathez G., Cailloux M., 1988, *A&A*, 191, L19
 Taylor A.N., Dye S., 1998, submitted to *MNRAS*
 Taylor A.N., Dye S., Broadhurst T.J., Benítez N., van Kampen E., 1998, *ApJ*, in press
 Wilson G., Cole S., Frenk C.S., 1996, *MNRAS*, 280, 199

APPENDIX A: PROOF THAT SPHERICAL LENSING POTENTIALS CANNOT HAVE

$$\gamma \propto \kappa^{1/2}$$

For spherically symmetric lensing potentials, both the lens convergence $\kappa(x)$ and magnification $\mu(x)$ are functions of the

deflection angle $\alpha(\mathbf{x})$ and its first derivative (eg. Schneider et al. 1992):

$$\kappa(x) = \frac{1}{2} \left(\frac{\alpha(x)}{x} + \frac{d\alpha(x)}{dx} \right), \quad (A1)$$

and

$$\begin{aligned} \mu^{-1}(x) &= \left(1 - \frac{\alpha(x)}{x}\right) \left(1 - \frac{d\alpha(x)}{dx}\right) \\ &= \left(\frac{1}{c} - \frac{\alpha(x)}{cx}\right) \left(c - c \frac{d\alpha(x)}{dx}\right). \end{aligned} \quad (A2)$$

So if we want to have $\mu^{-1} = (c^{-1} - \kappa)(c - \kappa)$ (e.g. eq. 21), we need to have the following two equalities:

$$\frac{\alpha(x)}{cx} = c \frac{d\alpha(x)}{dx} = \frac{1}{2} \left(\frac{\alpha(x)}{x} + \frac{d\alpha(x)}{dx} \right). \quad (A3)$$

Eliminating $d\alpha(x)/dx$, we have the following condition for the approximation $\gamma \propto \kappa^{1/2}$ to hold:

$$(c^2 - 2c + 1)\alpha(x) = 0. \quad (A4)$$

Besides the solution $\alpha(x) = 0$, corresponding to a sheet of matter, this condition is not met for any real c .